

Universal superconductivity phase diagram for pressurized tetradytite topological insulators

Shu Cai,^{1,4} S. K. Kushwaha,^{2,9} Jing Guo,¹ Vladimir A. Sidorov,³ Congcong Le,^{1,5} Yazhou Zhou,¹ Honghong Wang,^{1,4} Gongchang Lin,^{1,4} Xiaodong Li,⁶ Yanchuan Li,⁶ Ke Yang,⁷ Aiguo Li,⁷ Qi Wu,¹ Jiangping Hu,^{1,4} Robert J. Cava,^{2,*} and Liling Sun^{1,4,8,†}

¹Institute of Physics and Beijing National Laboratory for Condensed Matter Physics, Chinese Academy of Sciences, Beijing 100190, China

²Department of Chemistry, Princeton University, Princeton, New Jersey 08544, USA

³Institute for High Pressure Physics, Russian Academy of Sciences, 142190 Troitsk, Moscow, Russia

⁴University of Chinese Academy of Sciences, Beijing 100190, China

⁵Kavli Institute of Theoretical Sciences, University of Chinese Academy of Sciences, Beijing 100049, China

⁶Institute of High Energy Physics, Chinese Academy of Sciences, Beijing 100049, China

⁷Shanghai Synchrotron Radiation Facilities, Shanghai Institute of Applied Physics, Chinese Academy of Sciences, Shanghai 201204, China

⁸Songshan Lake Materials Laboratory, Dongguan, Guangdong 523808, China

⁹National High Magnetic Field Laboratory, LANL, Los Alamos, New Mexico 87504, USA



(Received 4 September 2018; published 13 November 2018)

We show that two different superconducting phases exist at high pressures in the optimized tetradytite topological insulators $\text{Bi}_2\text{Te}_2\text{Se}$ (BTS) and $\text{Bi}_{1.1}\text{Sb}_{0.9}\text{Te}_2\text{S}$ (BSTS). The superconducting phases emerge at structural phase transitions; the first at ~ 8.4 GPa for BTS and ~ 12.4 GPa for BSTS, and the second at 13.6 GPa for BTS and 20.4 GPa, for BSTS. Electronic structure calculations show that these phases do not have topological character. Comparison of our results with prior work on Bi_2Se_3 , Bi_2Te_3 , and $(\text{Bi}, \text{Sb})_2(\text{Se}, \text{Te})_3$ allows us to uncover a universal phase diagram for pressure-induced superconductivity in tetradytites, providing a basis for understanding the relationships between topological behavior, crystal structure, and superconductivity for these materials.

DOI: 10.1103/PhysRevMaterials.2.114203

I. INTRODUCTION

Tetradytites, well known as both thermoelectrics and topological insulators, have the general formula M_2X_3 , in which M is a group V metal, usually Bi or Sb, and X is a group VI anion, Te, Se or S. These elements have similar electronegativities, and thus the materials favor band inversion [1]. Theoretical and experimental work has shown that the electrons on their surfaces are topologically protected and can display remarkable properties [2–15], thus making tetradytites one of the most important materials families for the study of topological insulators (TIs). If made superconducting, then they are of interest for applications ranging from spintronic to quantum computation [2,16–18] motivating us to investigate how they might be tuned from a topological insulating state to a superconducting state.

Chemical doping is a commonly available tuning method. It can produce disorder, defects, and inhomogeneity in materials, however, and so is often not ideal. Pressure, on the other hand, is a clean way to realize the tuning of interactions in solids without introducing chemical complexity, and thus has been successfully adopted in the study of some topological insulators (TIs) [19–33]. Our study of the evolution of the topological surface states on optimized tetradytite $\text{Bi}_2\text{Te}_2\text{Se}$

(BTS) and $\text{Bi}_{1.1}\text{Sb}_{0.9}\text{Te}_2\text{S}$ (BSTS) crystals (by optimized we mean highest bulk resistivities at ambient pressure) at high pressures has been reported recently, for example [34]. Here we focus on the investigation of the pressure-induced superconductivity in these two materials. We find that two pressure-induced superconducting phases appear after their bulk insulating states are suppressed. By comparing our results with available data for pressurized Bi_2Se_3 [21,33], Bi_2Te_3 [23,31,35], and $(\text{Bi}, \text{Sb})_2(\text{Se}, \text{Te})_3$ [28], we find a universal pressure-dependent superconductivity phase diagram for all tetradytite TIs.

II. EXPERIMENTAL DETAILS

High-quality single crystals of BTS and BSTS were grown by the vertical Bridgman method, as described in Refs. [36,37]. Before the experiments, the crystals were freshly cleaved to expose pristine basal plane (001) surfaces.

The resistance measurements at high pressures were performed in a diamond anvil cell (DAC), in which diamond anvils with 400- μm flats and a nonmagnetic rhenium gasket with 100- μm -diameter hole were employed. The standard four-probe electrodes were applied on the cleavage plane of the BTS and the BSTS single crystals. To provide a quasihydrostatic pressure environment, NaCl powder was employed as the pressure medium. High-pressure x-ray diffraction (XRD) measurements were also performed in a DAC on beamline 4W2 at the Beijing Synchrotron Radiation Facility and on beamline 15U at the Shanghai Synchrotron Radiation

*Author to whom correspondence should be addressed:
rcava@Princeton.EDU

†llsun@iphy.ac.cn

Facility. Diamonds with low birefringence were selected for these XRD measurements. A monochromatic x-ray beam with a wavelength of 0.6199 Å was employed and silicon oil was employed as a pressure-transmitting medium. The pressure for all measurements in the DACs was determined by the ruby fluorescence method [38].

III. RESULTS AND DISCUSSION

In Fig. 1 we show the electrical resistance as a function of temperature for BTS and BSTS at pressures up to 24.1 and 31.8 GPa, respectively. As pressure increases, the resistances begin to drop near 2.1 K at about 8.4 GPa for BTS [Figs. 1(a) and Fig. S1 in the supplemental material] and near 2 K at about 12.4 GPa for BSTS [Figs. 1(c) and S1 in the supplemental material] [39]. The magnitude of these drops becomes more pronounced on further compression [Figs. 1(b) and 1(d)], and is followed by sharp decreases to zero resistance at 10.7 and 16 GPa [Fig. 1(d)], respectively. The observation of zero resistance is a signature of superconductivity. The superconducting transition temperatures T_C of these two materials exhibit identical pressure dependences—increases upon elevating pressure [Figs. 1(b) and 1(d)]. Remarkably, the T_{CS} of BTS and BSTS display a sudden rise at 13.6 and 20.4 GPa [see the red arrows in Figs. 1(b) and 1(d)], which implies the appearance of a new superconducting phase [21,24]. On further increase of the pressure, the T_C of the second superconducting phase decreases for both materials.

The superconductivity in these two TIs is confirmed by both high-pressure measurements of the ac susceptibility and the resistance under magnetic fields; the former shows diamagnetic throws [Figs. 2(a) and 2(b)] and the latter exhibits the magnetic field dependence of T_C displayed by superconductors (Fig. S2 in the supplemental material) [40]. In order to further differentiate the two superconductors, we estimate

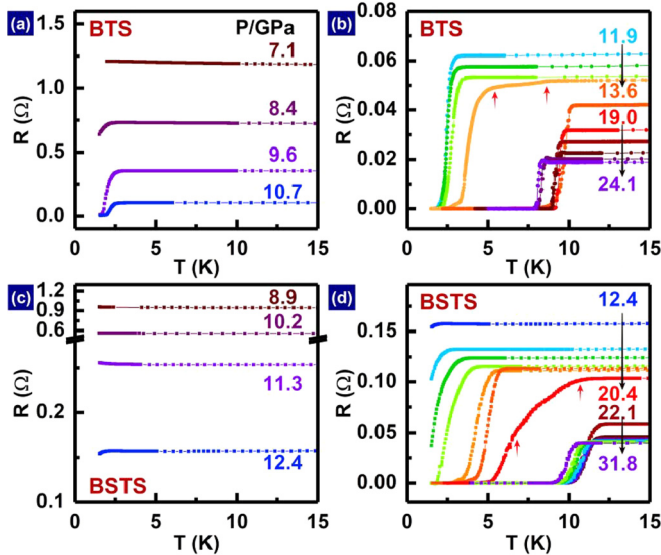


FIG. 1. Transport properties of BTS and BSTS at different pressures below 15 K. (a) and (b) display temperature dependence of electrical resistance obtained at different pressures for BTS. (c) and (d) show resistance as a function of temperature measured at different pressures for BSTS.

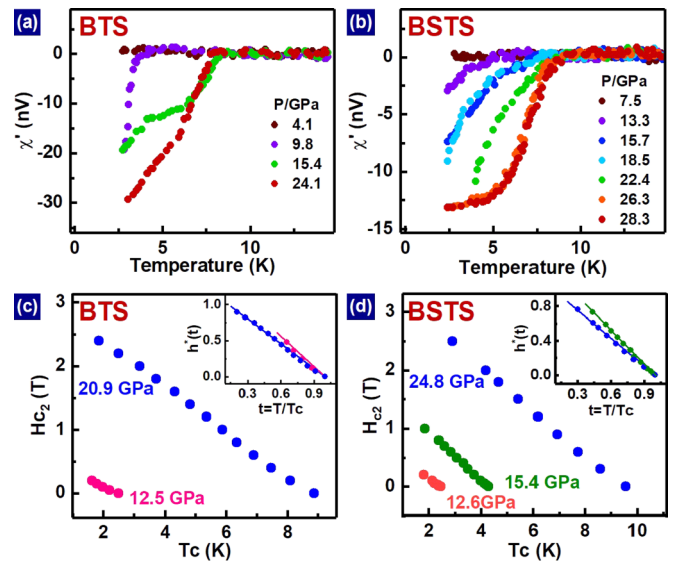


FIG. 2. Characterizations of pressure-induced superconductivity in BTS and BSTS. (a) and (b) show the results of high-pressure ac susceptibility measurements on BTS and BSTS, displaying diamagnetic throws at pressures where the samples show the zero resistance. (c) and (d) display upper critical field H_{C2} as a function of superconducting transition temperature T_C for pressurized BTS and BSTS. The estimated values of the upper critical fields of BTS at zero temperature are ~ 0.34 T at 12.5 GPa and 1.96 T at 20.9 GPa [Fig. 2(c)], while the H_{C2} values of BSTS are 0.57 T at 12.6 GPa, ~ 0.94 T at 15.4 GPa and 2.27 T at 24.8 GPa [Fig. 2(d)]. The normalized critical field $h^*(t)$ (here $h^*(t) = [H_{C2}(T)/T_C]/[dH_{C2}(T)/dT]|_{T=T_C}$) as a function of $t = T/T_C$ is also plotted for the two materials, displayed in the inset of Figs. 2(c) and 2(d). The data show that the $dh^*(t)/dt$ of the first superconducting phase of BTS subjected to 12.5 GPa has a different slope from that subjected to 20.9 GPa [inset of Fig. 2(c)], consistently demonstrating that pressure indeed induces two distinct superconducting phases in BTS. Similar behavior is also observed in BSTS [inset of Fig. 2(d)]. The $dh^*(t)/dt$ of the sample measured at 15.4 GPa is different from that measured at 24.8 GPa, suggesting that the two TIs investigated in this study show the same kinds of changes under high pressure.

The electronic state of topological insulators is protected by time-reversal symmetry [1,3,42,43] and therefore structural stability is one of the key issues for understanding the superconductivity found in the pressure range of our experiments. It is known that BTS maintains its tetradymite structure to 8 GPa [29,44], but there are no reports of the high-pressure structure of BSTS. Thus, we carried out high-pressure x-ray diffraction measurements on BSTS. Figure 3(a) presents the x-ray diffraction patterns collected at pressures up to 36.1 GPa

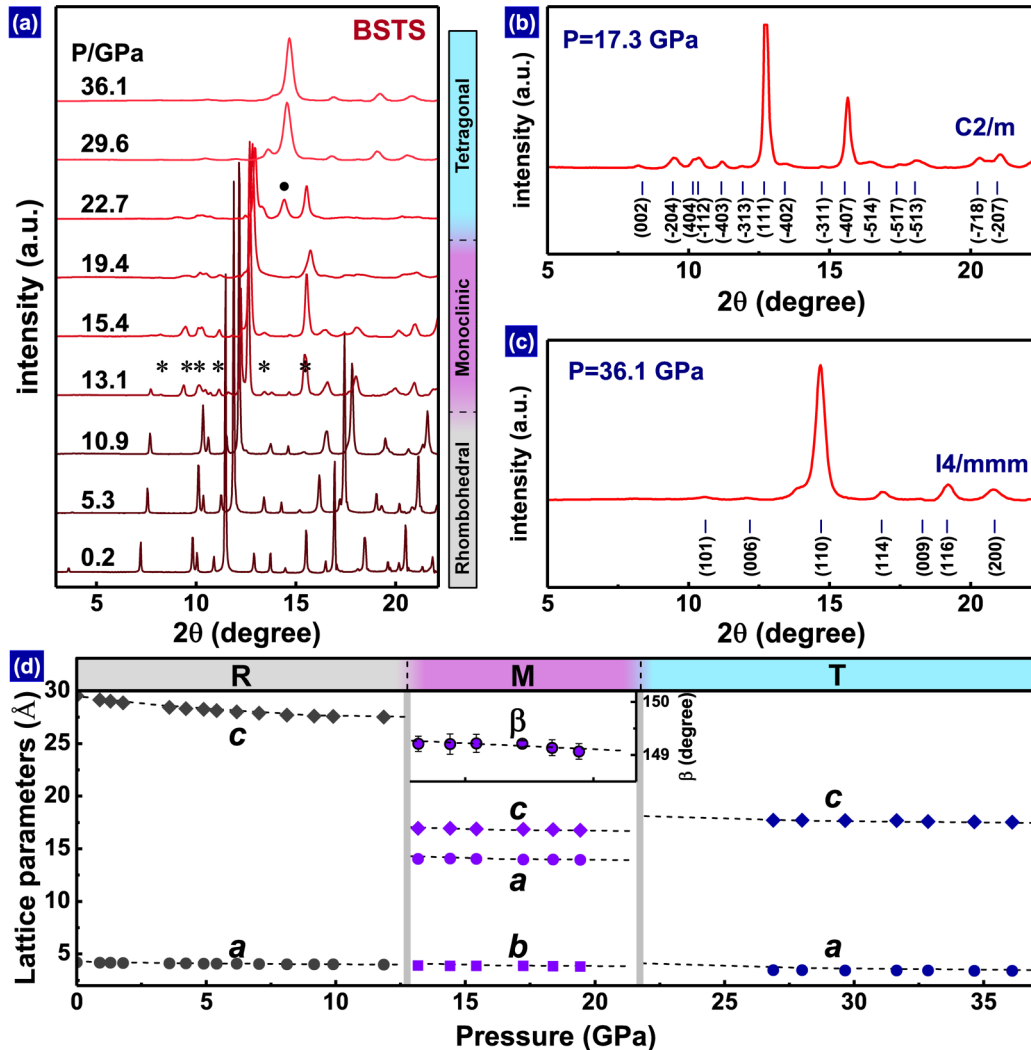


FIG. 3. Structural information for pressurized BSTS. (a) X-ray diffraction patterns collected at different pressures, displaying pressure-induced phase transitions at 13.1 GPa and 22.7 GPa. Stars (*) and the black solid dot in the figure indicate new peaks. (b) and (c) Refinements results on the new phases at 17.3 and 36.1 GPa, illustrating that they crystallize in monoclinic and tetragonal unit cells, respectively. (d) Pressure dependence of lattice parameters for rhombohedral (R), monoclinic (M), and tetragonal (T) phases.

for BSTS. Like other tetradytomite TIs, BSTS crystallizes in a rhombohedral (R) unit cell at ambient pressure [36,45] and maintains the R phase up to \sim 10.9 GPa. It then undergoes a structural phase transition at pressures between 10.9 and 13.1 GPa. The refinements for the high-pressure x-ray diffraction data collected at 17.3 GPa show that the high-pressure phase is monoclinic (M) in space group $C2/m$ [Fig. 3(b)]. On further increasing the pressure, BSTS converts into a tetragonal phase in space group $I4/mmm$ in the pressure range of 22.7–36.1 GPa [Fig. 3(c)]. The pressure dependence of lattice parameters in R, M, and T phases are presented in Fig. 3(d).

To investigate whether the superconducting phases found in pressurized BTS and BSTS still possess a nontrivial topological nature, we calculated the band structures for the M and T phases for BTS based on the high-pressure x-ray diffraction results [29]. Because the implied atomic disorder in the unit cell of BSTS makes the appropriate computations difficult, they were performed only for BTS. The calculations show that these two superconducting phases lose their topological

nature due to the structural phase transitions under pressure (Figs. S3, S4, and Table I in the supplemental material) [46–54]. The universal superconductivity behavior that we observe experimentally (see below) implies that the computed character of BTS can be applied for all tetradytomite TIs, with differences in carrier concentration and disorder, of course.

We summarize our high-pressure experimental results on BTS and BSTS in the pressure-temperature phase diagrams [Figs. 4(a) and 4(b)]. It is seen that these two TIs show the same type of behavior under pressure. There are three distinct ground states in the diagrams: the topological insulating state and the two superconducting states with distinct crystal structures. The first superconducting (SC-I) phase emerges in the monoclinic (M) phase, and its maximum T_C is about 3.1 K for BTS and 6 K for the BSTS. At pressure above 17.1 GPa (BTS) and 22.1 GPa (BSTS), the second superconducting (SC-II) phase with tetragonal (T) structure is found. The maximum T_C value of the SC-II phase is almost two times higher than that of SC-I phase, indicating that the T phase has a higher T_C in the these materials.

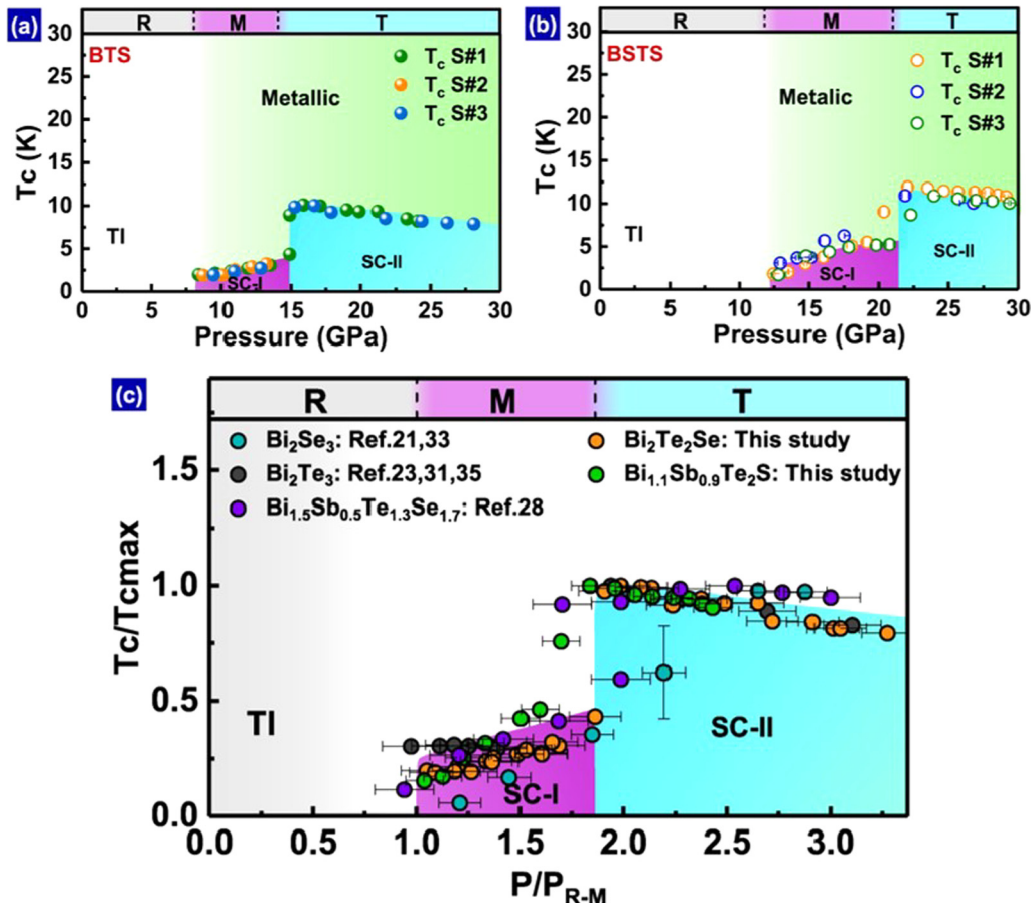


FIG. 4. Pressure-temperature phase diagrams of tetradymite TIs. (a) and (b) Pressure versus superconducting transition temperature T_c for BTS and BSTS, respectively. The acronym TI stands for the topological insulating state. SC-I and SC-II represent superconducting states with distinct crystal structures. R, M, and T stand for rhombohedral, monoclinic, and tetragonal phases, respectively. S#1, S#2, and S#3 represent samples 1, 2, and 3. (c) Plot of P/P_{R-M} and $T_c/T_{c\max}$ for Bi_2Te_3 , Bi_2Se_3 , $(\text{Bi}, \text{Sb})_2(\text{Se}, \text{Te})_3$, BTS, and BSTS, displaying a universal behavior for the tetradymite TIs.

Finally, we compare the normalized T_c -pressure phase diagrams for Bi_2Se_3 , Bi_2Te_3 and $(\text{Bi}, \text{Sb})_2(\text{Se}, \text{Te})_3$ with the results obtained in this study for BTS and BSTS. The normalization has been done using the observed phase transition pressures (The pressure of the rhombohedral to monoclinic transition for all materials is taken as 1 on the horizontal axis, and the maximum observed T_c for each material is taken as 1 on the vertical axis.) The phase diagrams reveal a remarkably universal character for all pressurized tetradymite TIs. As shown in Fig. S5, the SC-I phase for all the tetradymite TIs emerges at the appearance of the M phase and the SC-II phase develops at the appearance of the T phase. The critical pressures of the R to M and M to T transitions in different compounds are not the same, and the superconducting T_{cs} s are not the same, but if we normalize the pressures to P/P_{R-M} , and the superconducting transition temperatures to $T_c/T_{c\max}$, then a clear universal superconductivity phase diagram is revealed for all the members of the tetradymite family [Fig. 4(c)].

IV. CONCLUSION

In conclusion, we first find two pressure-induced superconducting phases in tetradymite topological insulators $\text{Bi}_2\text{Te}_2\text{Se}$

and $\text{Bi}_{1.08}\text{Sn}_{0.02}\text{Sb}_{0.9}\text{Te}_2\text{S}$ and demonstrate universal pressure dependent superconductivity phase diagrams for all the known tetradymite topological insulators. It is found that the SC-I phase emerges in a monoclinic phase and the SC-II phase appears in a tetragonal phase. The T_c of the tetragonal superconducting phase is higher than that of the monoclinic superconducting phase. It is expected that the present work provides information that can lead to a unified understanding of the connection between crystal structure, topological character and superconductivity in pressurized tetradymites TIs.

ACKNOWLEDGMENTS

We thank Professor Hongming Weng and Professor Qianghua Wang for helpful discussions. The work in China was supported by the National Key Research and Development Program of China (Grants No. 2017YFA0302900, No. 2016YFA0300300, and No. 2017YFA0303103), the NSF of China (Grants No. 11427805, No. U1532267, and No. 11604376), and the Strategic Priority Research Program (B) of the Chinese Academy of Sciences (Grant No. XDB25000000). The work at Princeton was supported by the ARO MURI on Topological Insulators, Grant No. W911NF-12-1-0461.

- [1] J. P. Heremans, R. J. Cava, and N. Samarth, *Nat. Rev. Mater.* **2**, 17049 (2017).
- [2] M. Z. Hasan and C. L. Kane, *Rev. Mod. Phys.* **82**, 3045 (2010).
- [3] Y. Xia, D. Qian, D. Hsieh, L. Wray, A. Pal, H. Lin, A. Bansil, D. Grauer, Y. S. Hor, R. J. Cava, and M. Z. Hasan, *Nat. Phys.* **5**, 398 (2009).
- [4] B. A. Bernevig, T. L. Hughes, and S. C. Zhang, *Science* **314**, 1757 (2006).
- [5] C. L. Kane and E. J. Mele, *Phys. Rev. Lett.* **95**, 146802 (2005).
- [6] M. König, S. Wiedmann, C. Brüne, A. Roth, H. Buhmann, L. Molenkamp, X.-L. Qi, and S.-C. Zhang, *Science* **318**, 766 (2007).
- [7] L. Fu, C. L. Kane, and E. J. Mele, *Phys. Rev. Lett.* **98**, 106803 (2007).
- [8] Y. Ando, *J. Phys. Soc. Jpn.* **82**, 102001 (2013).
- [9] X.-L. Qi and S.-C. Zhang, *Rev. Mod. Phys.* **83**, 1057 (2011).
- [10] Y. L. Chen, J. G. Analytis, J.-H. Chu, Z. K. Liu, S.-K. Mo, X. L. Qi, H. J. Zhang, D. H. Lu, X. Dai, Z. Fang, S. C. Zhang, I. R. Fisher, Z. Hussain, and Z.-X. Shen, *Science* **325**, 178 (2009).
- [11] Y.-S. Fu, M. Kawamura, K. Igarashi, H. Takagi, T. Hannaguri, and T. Sasagawa, *Nat. Phys.* **10**, 815 (2014).
- [12] D. Hsieh, Y. Xia, D. Qian, L. Wray, J. H. Dil, F. Meier, J. Osterwalder, L. Patthey, J. G. Checkelsky, N. P. Ong, A. V. Fedorov, H. Lin, A. Bansil, D. Grauer, Y. S. Hor, R. J. Cava, and M. Z. Hasan, *Nature (London)* **460**, 1101 (2009).
- [13] D. Hsieh, Y. Xia, D. Qian, L. Wray, F. Meier, J. H. Dil, J. Osterwalder, L. Patthey, A. V. Fedorov, H. Lin, A. Bansil, D. Grauer, Y. S. Hor, R. J. Cava, and M. Z. Hasan, *Phys. Rev. Lett.* **103**, 146401 (2009).
- [14] K. Miyamoto, A. Kimura, T. Okuda, H. Miyahara, K. Kuroda, H. Namatame, M. Taniguchi, S. V. Eremeev, T. V. Menshchikova, E. V. Chulkov, K. A. Kokh, and O. E. Tereshchenko, *Phys. Rev. Lett.* **109**, 166802 (2012).
- [15] M. Neupane, S.-Y. Xu, L. A. Wray, A. Petersen, R. Shankar, N. Alidoust, C. Liu, A. Fedorov, H. Ji, J. M. Allred, Y. S. Hor, T.-R. Chang, H.-T. Jeng, H. Lin, A. Bansil, R. J. Cava, and M. Z. Hasan, *Phys. Rev. B* **85**, 235406 (2012).
- [16] A. Kitaev, *Ann. Phys. (NY)* **303**, 2 (2003).
- [17] F. Wilczek, *Nat. Phys.* **5**, 614 (2009).
- [18] C. Nayak, S. H. Simon, A. Stern, M. Freedman, and S. Das Sarma, *Rev. Mod. Phys.* **80**, 1083 (2008).
- [19] X. Xi, C. Ma, Z. Liu, Z. Chen, W. Ku, H. Berger, C. Martin, D. B. Tanner, and G. L. Carr, *Phys. Rev. Lett.* **111**, 155701 (2013).
- [20] Y. H. Zhou, X. L. Chen, R. R. Zhang, J. F. Shao, X. F. Wang, C. An, Y. Zhou, C. Y. Park, W. Tong, L. Pi, Z. R. Yang, C. J. Zhang, and Y. H. Zhang, *Phys. Rev. B* **93**, 144514 (2016).
- [21] K. Kirshenbaum, P. S. Syers, A. P. Hope, N. P. Butch, J. R. Jeffries, S. T. Weir, J. J. Hamlin, M. B. Maple, Y. K. Vohra, and J. Paglione, *Phys. Rev. Lett.* **111**, 087001 (2013).
- [22] R. Vilaplana, D. Santamaría-Pérez, O. Gomis, F. J. Manjón, J. González, A. Segura, A. Muñoz, P. Rodríguez-Hernández, E. Pérez-González, V. Marín-Borrás, V. Muñoz-Sanjose, C. Drasar, and V. Kucek, *Phys. Rev. B* **84**, 184110 (2011).
- [23] L. Zhu, H. Wang, Y. Wang, J. Lv, Y. Ma, Q. Cui, Y. Ma, and G. Zou, *Phys. Rev. Lett.* **106**, 145501 (2011).
- [24] R. L. Stillwell, Z. Jenei, S. T. Weir, Y. K. Vohra, and J. R. Jeffries, *Phys. Rev. B* **93**, 094511 (2016).
- [25] T. V. Bay, T. Naka, Y. K. Huang, H. Luigjes, M. S. Golden, and A. de Visser, *Phys. Rev. Lett.* **108**, 057001 (2012).
- [26] G. Liu, L. Zhu, Y. Ma, C. Lin, J. Liu, and Y. Ma, *J. Phys. Chem. C* **117**, 10045 (2013).
- [27] Yanmei Ma, G. Liu, P. Zhu, H. Wang, X. Wang, Q. Cui, J. Liu, and Yanming Ma, *J. Phys.: Condens. Matter* **24**, 475403 (2012).
- [28] J. R. Jeffries, N. P. Butch, Y. K. Vohra, and S. T. Weir, *J. Phys.: Conf. Ser.* **592**, 012124 (2015).
- [29] J. Zhao *et al.*, *Phys. Chem. Chem. Phys.* **19**, 2207 (2017).
- [30] J. R. Jeffries, A. L. Lima Sharma, P. A. Sharma, C. D. Spataru, S. K. McCall, J. D. Sugar, S. T. Weir, and Y. K. Vohra, *Phys. Rev. B* **84**, 092505 (2011).
- [31] K. Matsabayashi, T. Terai, J. S. Zhou, and Y. Uwatoko, *Phys. Rev. B* **90**, 125126 (2014).
- [32] A. M. Nikitin, Y. Pan, Y. K. Huang, T. Naka, and A. de Visser, *Phys. Rev. B* **94**, 144516 (2016).
- [33] Z. H. Yu, L. Wang, Q. Y. Hu, J. G. Zhao, S. Yan, K. Yang, S. Sinogeikin, G. D. Gu, and H.-K. Mao, *Sci. Rep.* **5**, 15939 (2015).
- [34] S. Cai, J. Guo, V. A. Sidorov, Y. Zhou, H. Wang, G. Lin, X. Li, Y. Li, K. Yang, A. Li, Q. Wu, J. Hu, S. K. Kushwaha, R. J. Cava, and L. Sun, [arXiv:1807.02000](https://arxiv.org/abs/1807.02000).
- [35] C. Zhang, L. Sun, Z. Chen, X. Zhou, Q. Wu, W. Yi, J. Guo, X. Dong, and Z. Zhao, *Phys. Rev. B* **83**, 140504(R) (2011).
- [36] S. K. Kushwaha, I. Pletikosic, T. Lian, A. Gynis, S. H. Lapidus, Y. Tian, H. Zhao, K. S. Burch, J. Lin, W. Wang, H. Ji, A. V. Fedorov, A. Yazdani, N. P. Ong, T. Villa, and R. J. Cava, *Nat. Commun.* **7**, 11456 (2016).
- [37] S. Jia, H. Ji, E. Climent-Pascual, M. K. Fuccillo, M. E. Charles, J. Xiong, N. P. Ong, and R. J. Cava, *Phys. Rev. B* **84**, 235206 (2011).
- [38] H.-K. Mao, J. Xu, and P. Bell, *J. Geophys. Res.* **91**, 4673 (1986).
- [39] See Supplemental Material at <http://link.aps.org/supplemental/10.1103/PhysRevMaterials.2.114203> for details of temperature dependence of resistance.
- [40] See Supplemental Material at <http://link.aps.org/supplemental/10.1103/PhysRevMaterials.2.114203> for details of magnetic field dependence of superconducting transition temperatures in BTS and BSTS.
- [41] N. R. Werthamer, E. Helfand, and P. C. Hohenberg, *Phys. Rev.* **147**, 295 (1966).
- [42] H. J. Zhang, C. X. Liu, X. L. Qi, X. Dai, Z. Fang, and S. C. Zhang, *Nat. Phys.* **5**, 438 (2009).
- [43] L. Fu and C. L. Kane, *Phys. Rev. B* **76**, 045302 (2007).
- [44] M. B. Nielsen, P. Parisiades, S. R. Madsen, and M. Bremholm, *Dalton Trans.* **44**, 14077 (2015).
- [45] T. Misawa, Y. Fukuyama, Y. Okazaki, S. Nakamura, N. Nasaka, T. Sasagawa, and N. H. Kaneko, *IEEE Trans. Instrum. Meas.* **66**, 1489 (2017).
- [46] See Supplemental Material at <http://link.aps.org/supplemental/10.1103/PhysRevMaterials.2.114203> for details of theoretical calculations.
- [47] J. G. Zhao, H. Z. Liu, L. Ehm, Z. Q. Chen, S. Sinogeikin, Y. S. Zhao, and G. D. Gu, *Inorg. Chem.* **50**, 11291 (2011).
- [48] J. Zhao, H. Liu, L. Ehm, D. Dong, Z. Chen, and G. Gu, *J. Phys.: Condens. Matter* **25**, 125602 (2013).

- [49] G. Kresse and J. Hafner, [Phys. Rev. B](#) **47**, 558 (1993).
- [50] G. Kresse and J. Furthmüller, [Phys. Rev. B](#) **54**, 11169 (1996).
- [51] G. Kresse and J. Forthmüller, [Comput. Mater. Sci.](#) **6**, 15 (1996).
- [52] H. J. Monkhorst and J. D. Pack, [Phys. Rev. B](#) **13**, 5188 (1976).
- [53] S. K. Kushwaha, Q. D. Gibson, J. Xiong, I. Pletikosic, A. P. Weber, A. V. Fedorov, N. P. Ong, T. Valla, and R. J. Cava, [J. Appl. Phys.](#) **115**, 143708 (2014).
- [54] J. L. Mi, M. Bremholm, M. Bianchi, K. Borup, S. Johnsen, M. Søndergaard, D. Guan, R. C. Hatch, P. Hofmann, and Bo. B. Iversen, [Adv. Mater.](#) **25**, 889 (2013).